



Elimination of Secondary Oxide Phases in CdTe Nanostructured Thin Films Prepared by Conventional Spray Pyrolysis, and the Influence of Thermal Annealing

Hosein Robatjazi¹ · Hosein Eshghi¹

Received: 21 February 2023 / Accepted: 9 May 2023 / Published online: 13 June 2023
© The Minerals, Metals & Materials Society 2023

Abstract

In this study, cadmium telluride (CdTe) thin films were prepared by conventional spray pyrolysis on glass substrates at different temperatures (250°C, 300°C, and 350°C). Field-emission scanning electron microscopy (FESEM) images demonstrated that the substrate temperature significantly affected the morphology and thickness of the grown layers. The Seebeck effect measurements showed that all the studied layers had *p*-type conductivity. X-ray diffraction and Raman spectroscopy results indicated that the layer grown at 350°C had better CdTe crystalline quality, although it still contained secondary oxide phase components (TeO₂, TeO₃, and CdTeO₃), consistent with the analysis of electrical resistance versus temperature data. To eliminate oxide phase components in this sample, we used the annealing process in the presence of N₂ gas flux for 1 h at two different temperatures, 400°C and 450°C. It was found that annealing at 400°C, the optimum annealing temperature, achieved the goal of eliminating secondary oxide phase components.

Keywords CdTe · thin films · spray pyrolysis · nanostructure · annealing

Introduction

Cadmium telluride (CdTe), a II-VI compound semiconductor,¹ has a high optical absorption coefficient in the visible light wavelength range and a direct narrow band gap (about 1.4–1.5 eV), making it a promising candidate as an efficient absorber in sunlight.^{2–4} In terms of electrical conductivity, this semiconductor can behave as a *p*-type or *n*-type material, depending on either the lack of Cd atoms or excess Te acting as acceptor-like defects or the lack of Te atoms acting as donor-like defects in the grown layer.⁵ The CdTe thin films can be produced in hexagonal and/or cubic crystalline structures.⁶ This semiconductor has been widely used in optoelectronic devices such as photodiodes and photocapacitors,⁷ light-emitting diodes and field effect transistors,⁸ infrared (IR) windows, and solar cells.⁹ Fabrication of

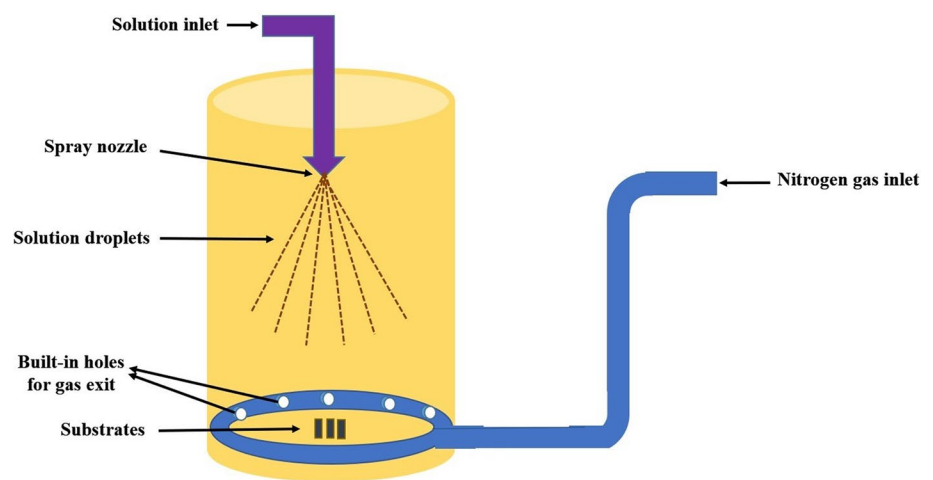
CdTe layers consisting of nanostructures such as nanorods or nanodots was found to improve the efficiency of these tools due to the high surface area available for light interactions.¹⁰

Various deposition methods have been used to prepare CdTe thin films, including electrodeposition,¹¹ pulsed laser deposition (PLD),¹² physical vapour deposition (PVD),¹³ electron beam evaporation,¹⁴ chemical bath deposition,¹⁵ vacuum evaporation,¹⁶ closed-space sublimation,¹⁷ radio-frequency (RF) magnetron sputtering,¹⁸ and spray pyrolysis.¹⁹ Among these, spray pyrolysis is cheaper than other methods and can grow layers on extended surface areas. By using this method, the impact of various growth parameters on the physical properties of the synthesised thin layers can be studied.²⁰ Gunjal et al.²¹ reported the synthesis of a thin CdTe layer using a “closed” chamber spray pyrolysis unit in a nitrogen atmosphere. Through this investigation, they grew a layer with relatively high purity (i.e., cubic phase polycrystalline structure) and a dense particle morphology. Ison et al.¹⁹ investigated the physical properties of CdTe films grown by a “closed” spray pyrolysis system using different ambient conditions, including ordinary laboratory ambient, partially evacuating the deposition chamber, and purging the chamber with nitrogen gas before the deposition. They reported that the environmental chemical composition

✉ Hosein Eshghi
h_eshghi@shahroodut.ac.ir
Hosein Robatjazi
hosseinrb94@gmail.com

¹ Faculty of Physics, Shahrood University of Technology, Shahrood, Iran

Fig. 1 Schematic of the home-designed spray apparatus chamber including a circular tube around the substrate for nitrogen gas inlet during the growth process.

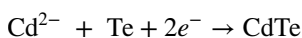
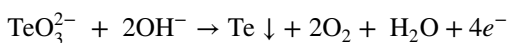


influences the phase purity of the layers, which are in fact a mixture of oxides (CdTeO_3 , TeO_2) and pure CdTe.

Accordingly, despite the above reports related to the synthesis of CdTe thin films using “closed spray pyrolysis systems,” to the best of our knowledge, we found no previous investigation in the literature on the influence of the substrate temperature on the morphological, structural, optical, and electrical properties of the CdTe thin films using a cost-effective “conventional spray pyrolysis unit” (Fig. 1), followed by an annealing process to achieve phase purity together with crystalline quality.

Experimental Details

The CdTe thin films were prepared by conventional spray pyrolysis on a glass substrate. The substrates were first washed in a double-distilled water and ethanol solution in an ultrasonic device and then dried with nitrogen gas. The spray precursor was prepared from a mixture of two solutions: 40 mM cadmium chloride hydrate ($\text{CdCl}_2 \cdot \text{H}_2\text{O}$) in 25 ml double-distilled water; 40 mM tellurium dioxide (TeO_2) in 20 ml ammonia solution; 3 ml hydrazine hydrate (reducing agent); and 2 ml hydrochloric acid (HCl). Cadmium telluride thin film deposition on the glass substrate is expected to occur after the chemical thermal reaction²⁰:



This chemical reaction leaves a solid coating of CdTe particles on the substrate. Notably, before deposition, the spray apparatus chamber was exposed to nitrogen gas with a purity of 99.9% for 10 min. In this study, we first prepared three samples at different substrate temperatures

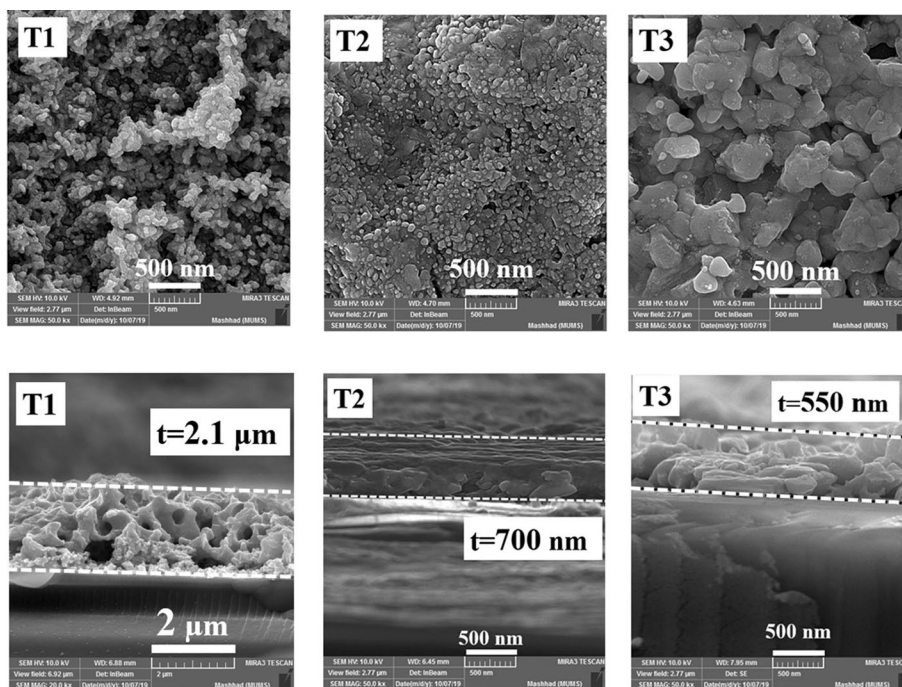
of 250°C, 300°C, and 350°C, labelled T1, T2, and T3, respectively (other deposition parameters are listed in Table I). Then, in the following, the best crystalline quality sample, belonging to the highest substrate temperature, was annealed in N₂ gas, as described in the “Annealing process” section.

This investigation examined the synthesised thin films using various techniques. The samples’ surface morphology was characterised using field emission scanning electron microscopy (FESEM, MIRA3 TESCAN). Structural characterization was carried out by an x-ray diffractometer (XRD, Bruker AXS), with spectral line emission CuK α 1.5404 Å. Raman measurements were studied using the uRaman-532-Ci system equipped with a 532-nm wavelength laser. A UV–visible double-beam spectrophotometer (Shimadzu UV–Vis 1800) in the wavelength range of 300–1100 nm was used for optical characterizations, and the Behpajoooh-BHP2063t potentiometer system was used for electrical measurements (I–V and R vs. T) of the samples under dark conditions, at room temperature, and at higher temperatures (up to 100°C). Finally, a home-built Seebeck effect apparatus was used to study the layers’ thermoelectric properties.

Table I The growth parameters used during CdTe film deposition

Process parameter	Value
Solution volume	50 ml
Solution concentration	40 mM
Spray gun nozzle–substrate distance	32 cm
Carrier gas pressure (dry air)	2 bar
Solution flow rate	5 ml/min
Nitrogen gas flow through film growth	750 sccm

Fig. 2 FESEM images (top and cross section views) of CdTe samples synthesised at different substrate temperatures (250°C, 300°C, and 350°C), i.e., samples T1, T2, and T3, respectively.



Results and Discussion

Effect of Substrate Temperature

Surface Morphology

Figure 2 shows the FESEM images of the grown samples at different substrate temperatures. The top views illustrate the surface morphology, and the side views present the cross-section and thickness of the layers. According to top-view images, in T1, the surface is rough and covered with particles of about 50–70 nm in diameter; in T2, the grains are joined together and make a relatively flat surface; and finally, in T3, the surface is covered with columnar-shaped configurations made of relatively large-sized nanoplates of about 150–200 nm. These results show that the morphology of the layers is very sensitive to the growth temperature. From cross-sectional images, it is apparent that by increasing the substrate temperature, the thickness of the layers decreases (from 2.1 μm to 700 nm and 550 nm). This trend in reduction in thickness with an increment of the substrate temperature is expected because, by increasing the substrate temperature, the tiny sprayed droplets suffer an upward flow of air, barely reaching the substrate and solidifying into a thin film.

Structural Properties

Figure 3 shows the XRD diffractograms of the synthesised layers together with the standard card pattern of the CdTe

cubic phase (JCPDS: 15-0770). As is evident in T1 and T2, the CdTe-related peaks are very weak, and the diffracted patterns are mainly related to Te (JCPDS 04-0554) and/or TeO_2 (JCPDS 52-1005) as marked by (*), as well as CdTeO_3 (JCPDS 77-1906) marked by (●) as the secondary phases.¹⁴ But in T3, both the high-intensity peaks, i.e., (111), (220), and (311), and the low-intensity peaks, (400), (331), (422), and (511), are well-matched with the polycrystalline CdTe cubic structure. From a phase purity point of view, although T3 is not ideal, as evident compared to the other

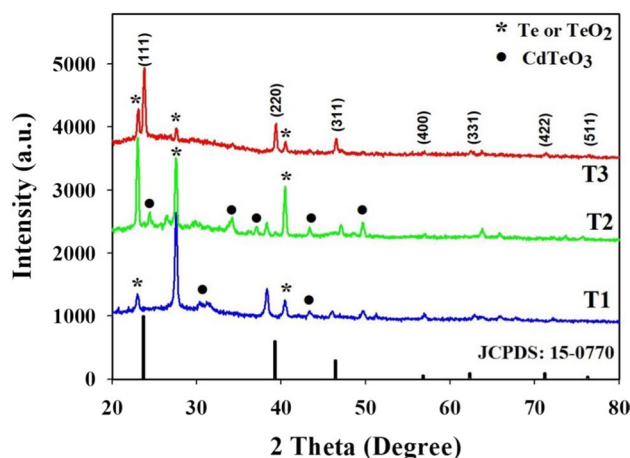


Fig. 3 XRD diffractograms of the synthesised layers grown at different substrate temperatures; together with CdTe standard card cubic phase peak positions.

two samples, the growth conditions in this layer have led to minimal CdTeO₃ compound.

For a detailed analysis of the structural properties in T3, we have calculated parameters including crystallite size (D), dislocation density (δ), microstrain (ϵ), inter-planar distance (d), and lattice parameter (a) related to the cubic structure of CdTe for the (111) preferred peak using the following equations^{21–24}:

$$D = 0.9\lambda/\beta \cos \theta \quad (1)$$

$$\delta = 1/D^2 \quad (2)$$

$$\epsilon = \lambda/D \sin \theta - \beta/\tan \theta \quad (3)$$

$$2d_{hkl} \sin \theta_{hkl} = n\lambda \quad (4)$$

$$a = d\sqrt{h^2 + k^2 + l^2} \quad (5)$$

where β is the full width at half maximum (FWHM in radians), D is the crystallite size, θ is the Bragg angle, λ is the wavelength of x-ray radiation, d is the inter-planar distance, and a is the lattice parameter. The results are presented in Table II. According to these results, the average crystallite size in this sample is about 27.5 nm. In addition, the values of d and a are compatible with those of the standard values as in the standard card (JCPDS: 15-0770).

Figure 4 shows the Raman spectra of the studied samples in the wavelength range of 100–800 cm⁻¹. The spectra contain several peaks at 119 cm⁻¹, 140 cm⁻¹, 163 cm⁻¹, 263 cm⁻¹, and 557 cm⁻¹. The first peak (119 cm⁻¹) is assigned to the A1 phonon vibration modes of the hexagonal Te structure due to the presence of Te-excess atoms in the lattice.²⁵ The second and third peaks (140 cm⁻¹ and 163 cm⁻¹) correspond to the transverse optic (TO) and longitudinal optic (LO) phonon modes in the CdTe lattice, respectively. The fourth peak, located at 263 cm⁻¹ is associated with the surface roughness of the layers.²¹ Finally, the fifth peak, positioned at 557 cm⁻¹, is assigned to the formation of the TeO₃ phase.²⁶ These data show that increasing the substrate temperature decreases the relative intensity of the oxide-related peak, i.e., 557 cm⁻¹.

Electrical and Thermoelectric Properties

Figure 5a shows the ohmic characteristics of current–voltage (I–V) measurements of the studied samples in the voltage range of –3 to +3 V. As seen, T3 has the highest electrical resistance (3.61 M Ω). In contrast, T1 and T2 have much smaller values of 3.7 k Ω and 1.45 k Ω , respectively (about three orders of magnitude). This enormous variation in electrical resistance could be due to the reduction of secondary phase components (such as Te, TeO₂ and CdTeO₃) in the CdTe network with increased growth temperature. We have performed the Seebeck effect measurement to recognise the nature of the conductivity (either n - or p -type) of these samples. All samples showed that thermoelectric voltage at the cold end was higher than at the hot end, confirming the p -type conductivity of these layers. Based on Seebeck theory (Eq. 6), it is clear from Fig. 5b that as the temperature difference between the two ends of the layers increases, the absolute values of the thermoelectric voltage differences increase linearly.

$$V = S\Delta T \quad (6)$$

where S is the Seebeck coefficient in volts/C^o, this quantity depends on material properties and temperature. Considering Eq. 6, the analysis provides the Seebeck coefficients of 0.032 mV/C^o, 0.029 mV/C^o, and 0.152 mV/C^o in T1, T2, and T3, respectively. According to the thermoelectric theory of materials,²⁷ the amount of the Seebeck coefficient is expected to be directly related to the electrical resistivity

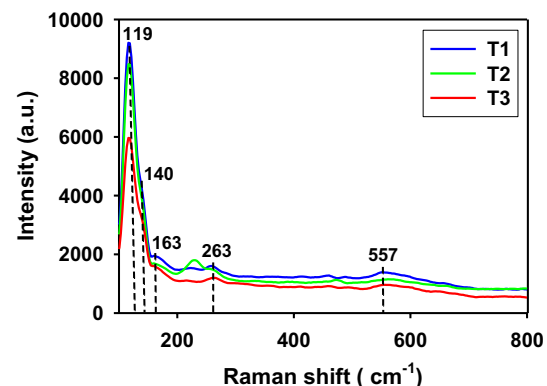


Fig. 4 Raman spectra of the synthesised CdTe samples.

Table II Structural analysis of the CdTe compound for (111) preferred cubic structure direction in T3 before and after annealing

Sample	2 θ ($^{\circ}$)	FWHM ($^{\circ}$)	D (nm)	$\delta \times 10^{-2}$ nm ⁻²	$\epsilon \times 10^{-3}$	d_{hkl} (\AA)		a (\AA)	
						Obs	Stand	Obs	Stand
T3	23.80	0.294	27.5	0.132	2.86	3.734	3.766	6.467	6.483
T3-400	23.78	0.148	55.5	0.0325	1.23	3.737	3.766	6.472	6.483
T3-450	23.68	0.198	44.1	0.0592	1.87	3.752	3.766	6.499	6.483

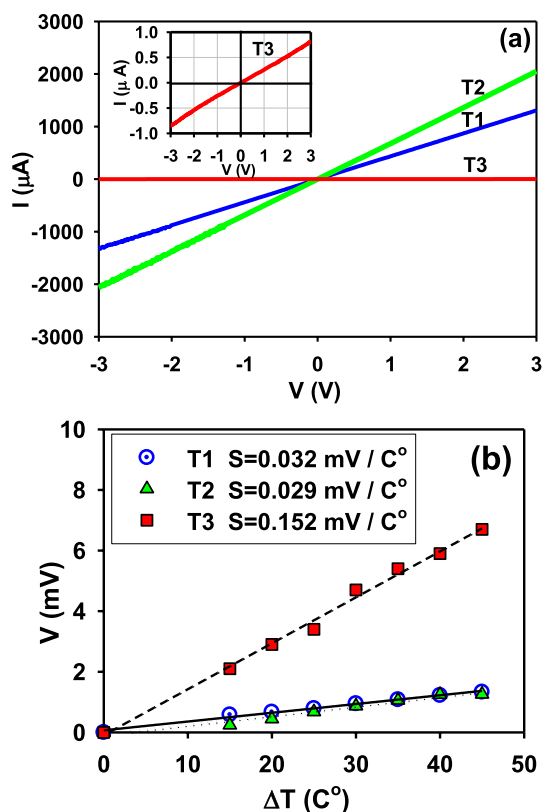


Fig. 5 (a) Current–voltage (I – V) characteristics of investigated samples; for clarity, the inset shows the current–voltage variations in T3 alone; (b) the Seebeck effect measurements in synthesised samples.

of the sample. As is evident, this relationship is well consistent with the measured electrical resistance of these samples.

As shown in Fig. 6a and b, we measured the temperature dependence of electrical resistance (R – T) of the samples to determine the average energy position of native acceptor-like defect level(s) inside the band gap relative to the valence band edge (VBE). As seen with increasing temperature, the electrical resistance of the layers decreases.²⁸ In p -type semiconductor materials, this behaviour can be attributed to the thermal excitation of electrons from the VBE to higher energy defect levels, resulting in the transfer of energy known as the average thermal activation energy (E_a). This quantity can be obtained from the Arrhenius equation²⁹:

$$R = R_0 \exp(E_a/kT) \quad (7)$$

where R is the sample resistance at temperature T , R_0 is a constant, E_a is the average thermal activation energy (here, relative to the VBE), and k is the Boltzmann constant ($8.625 \cdot 10^{-5}$ eV/K). Figure 6c and d shows the detailed analysis considering $\ln(R)$ versus $1000/T$ plots. The slope of the linear fit to these data is expected to be proportional to E_a . Our analysis shows that with increasing substrate

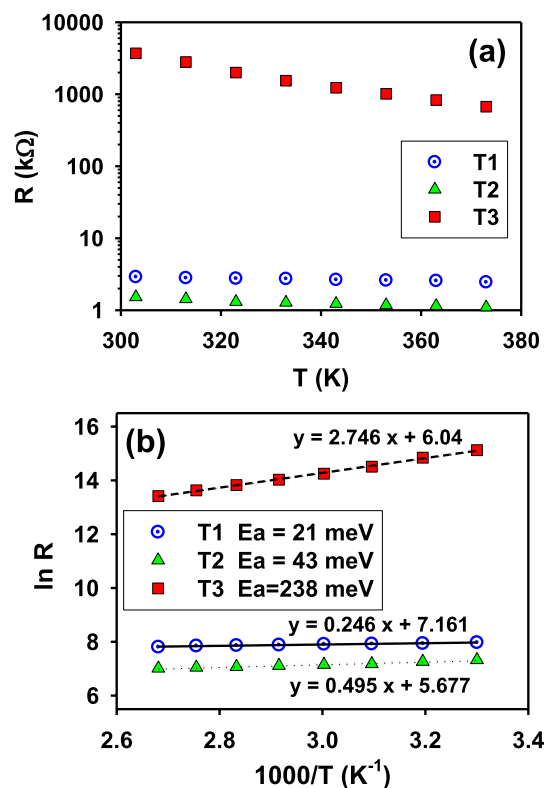


Fig. 6 (a) Variations of electrical resistance versus temperature for the studied samples; (b) theoretical analysis for thermal activation energy evaluation, using Eq. 7.

temperature, the average activation energy of the layers gradually increases from 21 meV to 43 meV in T1 and T2, and 238 meV in T3. The smaller E_a values could be due to native oxide levels corresponding to oxide compositions (TeO_2 , TeO_3 , and CdTeO_3) and their energy separations from VBE, while the bigger one, as discussed in the “[Electrical and Thermoelectric Properties](#)” section, is shifted towards native defects in the CdTe crystal lattice.

Optical Properties

Figure 7a and b show the transmittance (T) and absorbance (a) spectra of the studied thin films. It is evident that increasing the substrate temperature and, therefore, the layer thicknesses (t), along with different morphologies (“[Surface Morphology](#)” section), has led to an enhancement in the transmittance of the layers. In contrast, their corresponding absorbance has decreased, which is compatible with Beer’s law: $T = \exp(-\alpha t)$. Knowing the absorbance spectrum, we have evaluated the direct optical band gap (E_g) of the layers using the Tauc relation²¹:

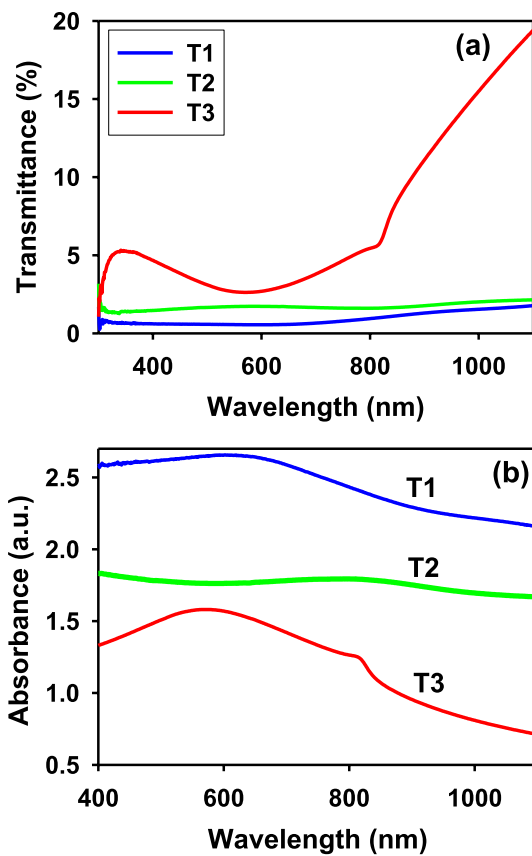


Fig. 7 (a) Transmittance and (b) optical absorbance spectra of the samples T1, T2, and T3, prepared at different substrate temperatures.

$$(ah\nu)^2 = A(h\nu - E_g) \quad (8)$$

where A is a constant and $h\nu$ is the photon energy. Analysis showed the E_g values varied from about 1.1 eV to 1.2 eV and finally to 1.37 eV as the substrate temperature increased. These variations could be due to the structural phase compositions and defect densities of the layers. The E_g value related to T3 shows the closest value to CdTe composition, i.e., 1.4 eV.¹⁴

Annealing Process

To achieve improved CdTe thin film crystallinity and to remove the secondary composition phases, we proceeded with our investigation on T3 by annealing for a period of 1 h in a 20 sccm N_2 gas flux atmosphere at two different temperatures of 400°C and 450°C, labelled as T3-400 and T3-450, respectively.

Surface Morphology

Figure 8 shows the FESEM images of T3 before and after annealing. As evident, increasing the annealing temperature

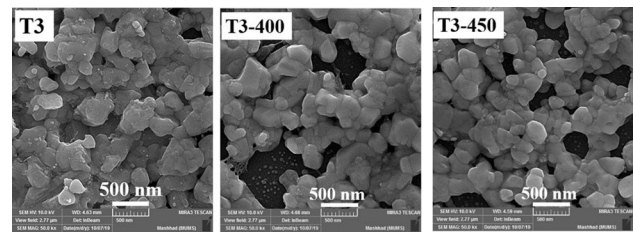


Fig. 8 FESEM images of sample T3 before and after annealing at 400°C and 450°C, labeled as T3-400 and T3-450, respectively.

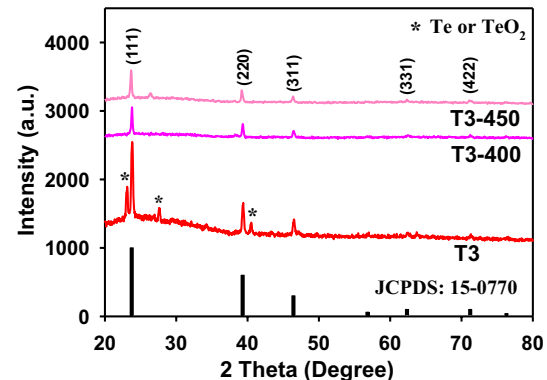


Fig. 9 XRD diffractograms of sample T3, before and after annealing processes.

while the constituent grains are highly packed increases their average sizes (~ 200 – 250 nm).

Structural Properties

Figure 9 shows the XRD diffractograms of the annealed samples and the standard pattern of the CdTe cubic phase (JCPDS: 15-0770). It is apparent that the related TeO_2 peaks are removed during the annealing process, leading to a better purified CdTe structure, especially at 400 °C. For further detailed structural analysis of the annealed samples, we used Eqs. 1–5 (Table II). These findings indicate that (1) the annealing process increased crystallite size while decreasing dislocation density and induced microstrains, and (2) the T3-400 sample has better crystallinity (larger crystallite size and smaller δ and ϵ) than the T3-450 sample.

Figure 10 shows the Raman spectra of T3 before and after annealing. These findings show that after annealing, the related oxygen-bond peak intensities, one at 119 cm^{-1} , assigned to Te-excess atoms and/or Te–O bonds, and the other at 557 cm^{-1} , assigned to the formation of the TeO_3 phase, are reduced, which is consistent with the XRD diffractograms (Fig. 9). This could be due to the fractional removal of the residual excess oxygen atoms in the lattice.

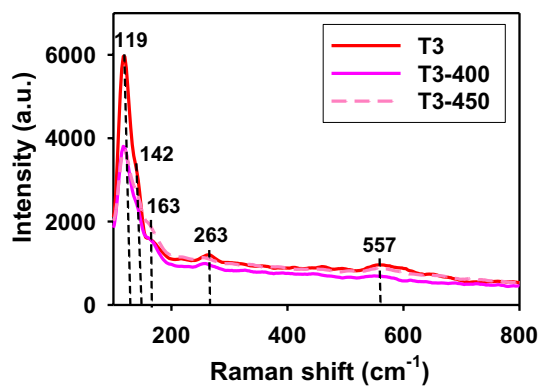


Fig. 10 Raman spectra of sample T3, before and after annealing at 400°C and 450°C.

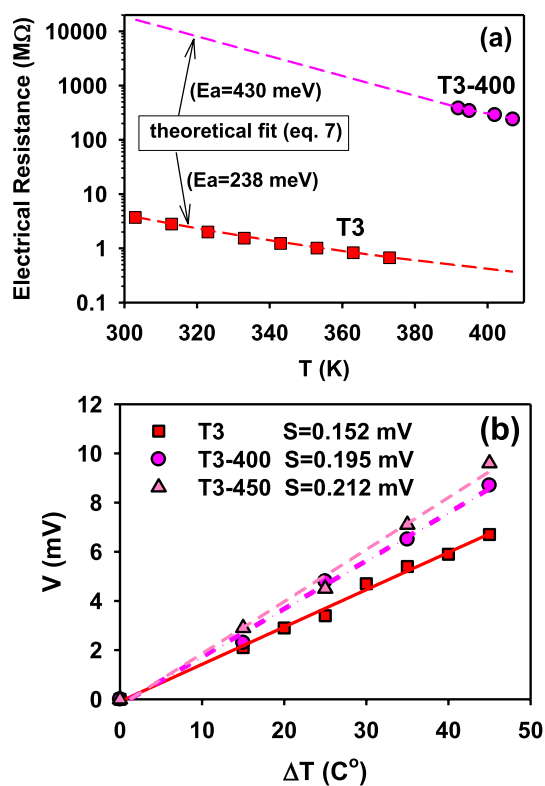


Fig. 11 (a) The variations of electrical resistance versus temperature in T3 and T3-400; (b) the Seebeck effect data and analysis of T3, before and after annealing.

Electrical and Thermoelectric Properties

Figure 11a shows the variations of electrical resistance versus temperature (390–410 K) in T3 and T3-400. It is clearly observed that no response was measured in T3-450 due to its very high resistance characteristic. Compared to T3, in T3-400, due to the reduction of oxide composition, the electrical resistance at a given temperature has appreciably

increased (about three orders of magnitude). Based on the Arrhenius model, Eq. 7, the estimated activation energy in this sample has been raised to about 430 meV, which is close to the reported value (460–500 meV) by Babkair et al.³⁰, which is attributed to the native crystal defects mainly due to deficiencies of Cd atoms in the CdTe crystal lattice.

In addition, we performed the Seebeck effect measurement for the annealed samples. The results are shown in Fig. 11b. We analysed these data and realised that while the annealed layers maintained their *p*-type conductivity nature, the Seebeck coefficient (*S*) (Eq. 6) increased from 0.152 in T3 to 0.195 mV/C° and 0.212 mV/C° in T3-400 and T3-450, respectively. As noted in Sect. 7, the trend in variations of *S* values is well matched with the trend in variations of electrical resistance in these layers.

Optical Properties

Figure 12a and b shows the optical transmittance and absorbance spectra of T3 before and after the annealing process. It is clear that after annealing, in the long wavelength range (above 830 nm), i.e., the transparency range, the amount of transmittance of the layers is increased so that T3-400 has a higher transmittance than T3 and T3-450. This could be due to fewer photon scattering mechanisms, including dislocations, grain boundaries, and structural phase inhomogeneity, in T3-400 compared to the other two samples. Considering the absorbance spectra, the direct band gap (E_g) of these samples is evaluated using the Tauc relation (Eq. 8), Fig. 12c. The incremental variations of E_g values in annealed samples could be due to structural phase purification, which leads to a decrement of defect density and, therefore, a band tail narrowing effect close to the VBE.

Conclusions

In the first step, CdTe thin films were deposited at different substrate temperatures (250°C, 300°C, and 350°C, labelled as T1, T2, and T3) by a conventional spray pyrolysis apparatus while applying N₂ gas flow at the bottom of the chamber. The FESEM images revealed that the substrate temperature significantly impacted the morphology and thickness of the grown layers (ranging from 2.1 μm to 550 nm). While Seebeck effect measurements showed that all the studied layers have *p*-type conductivity, the XRD diffractograms and Raman spectra revealed that, in addition to the CdTe cubic structure phase, there are also secondary phases of Te and Cd oxide phases (i.e., TeO₂, TeO₃, and CdTeO₃) in the synthesized layers, with the smallest amount in T3. To obtain a layer without oxide phase components, we tried using the annealing process in the presence of N₂ gas flux for one hour at two different temperatures of 400°C and 450°C. The

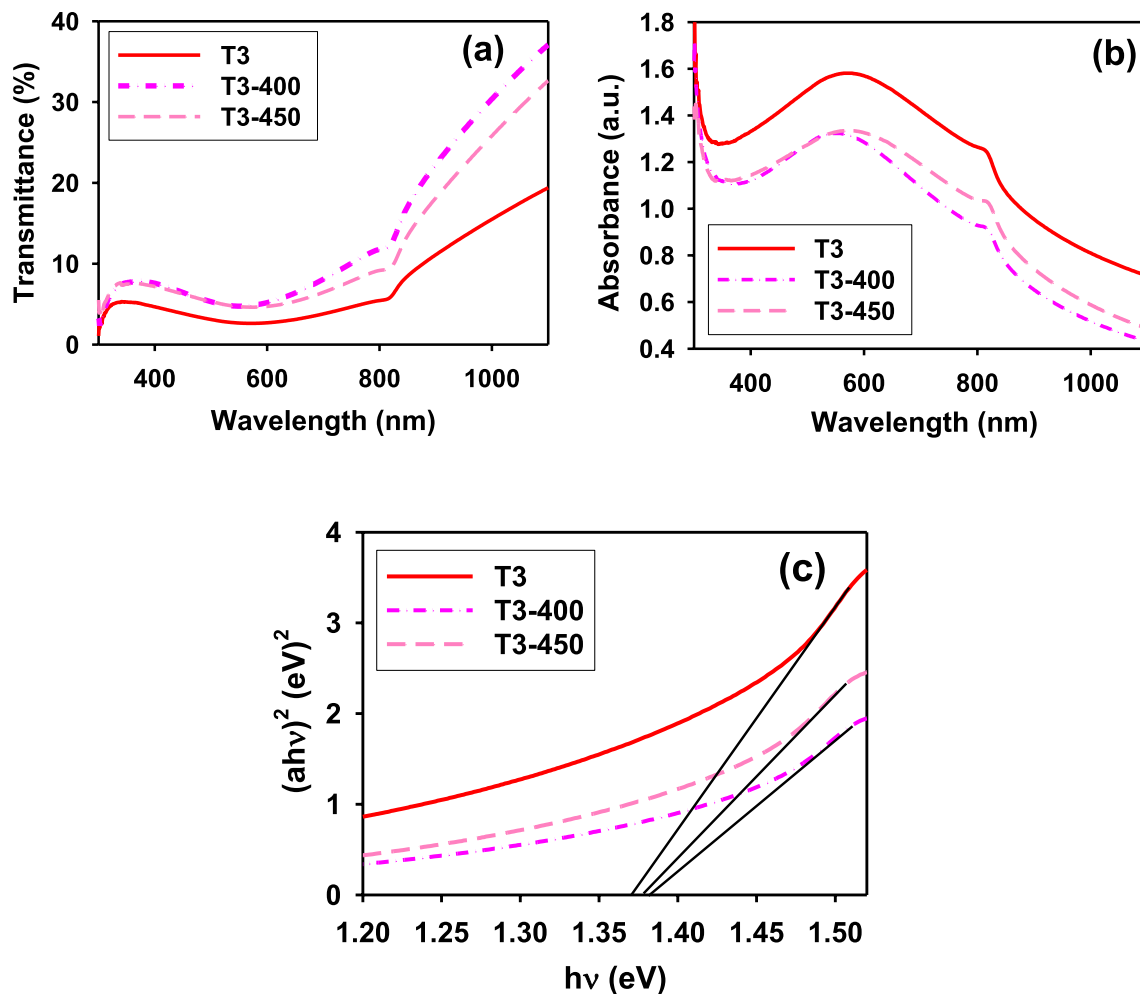


Fig. 12 (a) Transmittance and (b) optical absorbance spectra of T3, before and after annealing (T3-400 and T3-450); (c) energy gap analysis of the samples.

XRD diffractograms, Raman spectra, and estimated activation energy from the analysis of electrical resistance versus temperature data confirmed that annealing at 400 °C, the optimum annealing temperature, is sufficient to eliminate the secondary oxide phase components.

Conflict of interest On behalf of all authors, the corresponding author states that there is no conflict of interest.

References

1. M. Aven and J. Prener, *Physics and Chemistry of Two-Six Compounds* (Amsterdam: Elsevier 1967).
2. E. Akbarnejad, M. Ghoranneviss, and M.R. Hantehzadeh, Synthesis and characterization of CdTe nanostructures grown by RF magnetron sputtering method. *Eur. Phys. J. D* 71, 1 (2017).
3. E. Akbarnejad, M. Ghoranneviss, and A. Salar Elahi, Cadmium telluride nanostructure deposition by RF magnetron sputtering on flexible Cu foils. *J. Inorg. Organomet. Polym. Mater.* 26, 270 (2016).
4. K.V. Krishna and V. Dutta, Spray deposition of CdTe-Te thin films using ethylene-diamine-tetra-acetic acid as a complexing agent in the precursor solution. *Sol. Energy Mater. Sol. Cells* 80, 247 (2003).
5. E. Campos-González, F. de Moure-Flores, L.E. Ramírez-Velázquez, K. Casallas-Moreno, A. Guillén-Cervantes, J. Santoyo-Salazar, G. Contreras-Puente, and O. Zelaya-Angel, Structural and optical properties of CdTe-nanocrystals thin films grown by chemical synthesis. *Mater. Sci. Semicond. Process.* 35, 144 (2015).
6. V.V. Ison, A. Ranga Rao, and V. Dutta, Stabilization of hexagonal phase in spray-deposited CdTe films by the presence of electric field. *Sol. Energy Mater. Sol. Cells* 93, 1507 (2009).
7. A.S. Dahlan, A. Tataroğlu, A.A. Al-Ghamdi, S. Bin-Omran, Y. Al-Turku, F. El-Tantawy, and F. Yakuphanoglu, Photodiode and photocapacitor properties of Au/CdTe/p-Si/Al device. *J. Alloys Compd.* 646, 1151 (2015).
8. S. Chander and M.S. Dhaka, Physical properties of vacuum evaporated CdTe thin films with post-deposition thermal annealing. *Phys. E Low Dimens. Syst. Nanostruct.* 73, 35 (2015).

9. V.M. Nikale, S.S. Shinde, C.H. Bhosale, and K.Y. Rajpure, Physical properties of spray deposited CdTe thin films: PEC performance. *J. Semicond.* 32, 033001 (2011).
10. B. Luo, Y. Deng, Y. Wang, Y. Shi, L. Cao, and W. Zhu, Magnetron sputtering based direct fabrication of three dimensional CdTe hierarchical nanotrees exhibiting stable superhydrophobic property. *Appl. Surf. Sci.* 280, 550 (2013).
11. F. Golgovici and T. Visan, Electrodeposition behavior of CdTe from choline chloride-urea ionic liquids. *Chalcogenide Lett.* 9, 165 (2012).
12. D. Wang, Y. Yang, T. Guo, X. Xiong, Y. Xie, K. Li, B. Li, and M. Ghali, Effect of pulse bias voltages on performance of CdTe thin film solar cells prepared by pulsed laser deposition. *Sol. Energy* 213, 118 (2021).
13. T. Takamoto, T. Agui, H. Kurita, and M. Ohmori, Improved junction formation procedure for low temperature deposited CdS/CdTe solar cells. *Sol. Energy Mater. Sol. Cells* 49, 219 (1997).
14. S. Goyal and R.P. Chauhan, Substrate temperature dependent variation in the properties of cadmium telluride thin films deposited on glass. *J. Mater. Sci.: Mater. Electron.* 30, 1345 (2018).
15. L. Gouda, Y.R. Aniruddha, and S.K. Ramasesha, Correlation between the solution chemistry to observed properties of CdTe thin films prepared by CBD method. *J. Mod. Phys.* 3, 1870 (2012).
16. U. Chander and M.S. Dhaka, Preparation and physical characterization of CdTe thin films deposited by vacuum evaporation for photovoltaic applications. *Adv. Mater. Lett.* 6, 907 (2015).
17. M.N. Harif, K.S. Rahman, C. Doroody, H.N. Rosly, M. Isah, M.A. Alghoul, H. Misran, and N. Amin, Microstructural evolution of oxygen incorporated CdTe thin films deposited by close-spaced. *Mater. Lett.* 306, 130552 (2022).
18. E. Camacho-Espinosa, E. Rosendo, A.I. Oliva, T. Diaz, N. Carlos-Ramirez, and H. Juarez, Physical properties of sputtered CdTe thin films. *Indian J. Appl. Res.* 4, 588 (2014).
19. V.V. Ison, A. Ranga Rao, and V. Dutta, Characterization of spray deposited CdTe films grown under different ambient conditions. *Solid State Sci.* 11, 2003 (2009).
20. S. Tewari and A. Bhattacharjee, Synthesis and characterization of cadmium chalcogenide CdX (X = S, Te) thin films. *Int. J. Chem. Sci.* 7, 105 (2009).
21. S.D. Gunjal, Y.B. Kholam, S.R. Jadhkar, T. Shripathi, V.G. Sathe, P.N. Shelke, M.G. Takwale, and K.C. Mohite, Spray pyrolysis deposition of p-CdTe films: Structural, optical and electrical properties. *Sol. Energy* 106, 56 (2014).
22. S. Chander, Impact of thermal annealing on physical properties of vacuum evaporated polycrystalline CdTe thin films for solar cell applications. *Phys. E Low Dimens. Syst. Nanostruc.* 80, 62 (2016).
23. B. Fultz and J.M. Howe, *Transmission Electron Microscopy and Diffractometry of Materials*, (Berlin: Springer Publishing, 2012).
24. X. Yang, Y. Zhang, G. Xu, X. Wei, Zh. Ren, G. Shen, and G. Han, Phase and morphology evolution of bismuth ferrites via hydrothermal reaction route. *Mater. Res. Bull.* 48, 1694 (2013).
25. M. Maghouli and H. Eshghi, Studying the effect of deposition time on physical properties of CdTe thin films; influence of CdTe electrical properties on CdS/CdTe heterojunction rectifying behavior. *Optik* 218, 165132 (2020).
26. J. Carmona-Rodríguez, R. Lozada-Morales, O. Jiménez-Sandoval, F. Rodríguez-Melgarejo, M. Meléndez-Lira, and S.J. Jiménez-Sandoval, CdTeO_x to CdTeO₃ structural phase transition in as-grown polycrystalline films by reactive sputtering. *J. Appl. Phys.* 103, 123516 (2008).
27. N.W. Ashcroft and D.N. Mermin, *Solid State Physics*, (Philadelphia: Saunders College Publishing 1976).
28. A.U. Ubale, R.J. Dhokne, P.S. Chikhlikar, V.S. Sangawar, and D.K. Kulkarni, Characterization of nanocrystalline cadmium telluride thin films grown by successive ionic layer adsorption and reaction (SILAR) method. *Bull. Mater. Sci.* 29, 165 (2006).
29. R. Srivastava, Investigation on temperature sensing of nanostructured zinc oxide synthesized via oxalate route. *J. Sens. Technol.* 2, 8 (2012).
30. S. Babkair and A. Ansari, Activation energy and density of states of CdTe thin films from temperature dependent I–V measurements. *Mater. Chem. Phys.* 127, 296 (2011).

Publisher's Note Springer Nature remains neutral with regard to jurisdictional claims in published maps and institutional affiliations.

Springer Nature or its licensor (e.g. a society or other partner) holds exclusive rights to this article under a publishing agreement with the author(s) or other rightsholder(s); author self-archiving of the accepted manuscript version of this article is solely governed by the terms of such publishing agreement and applicable law.